Int. J. Solids Structures Vol. 25, No. 12, pp. 1411-1426, 1989
Printed in Great Britain.

0020-7683/89 $3.00+.00
© 1989 Pergamon Press plc

ANTISYMMETRICAL 3-D STRESS FIELD NEAR THE CRACK FRONT OF A THIN ELASTIC PLATE

T. NAKAMURA
Department of Mechanical Engineering, State University of New York at Stony Brook,
NY 11794, U.S.A.

and

D. M. PARKS
Department of Mechanical Engineering, Massachusetts Institute of Technology,
Cambridge, MA 02139, U.S.A.

(*Received* 14 *September* 1988)

Abstract—Based on detailed three-dimensional finite element analysis, the near-tip field of a thin elastic plate remotely subjected to Mode II antisymmetrical loading is investigated. The computed results show the transition to a three-dimensional state to occur near the radial distance from the crack tip of 1.5 times the plate thickness. In the close vicinity of the crack front, the asymptotic stress field is characterized by a combination of plane strain Mode II and anti-plane Mode III singular ($1/\sqrt{r}$) fields. The domain of such fields extends approximately 0.5% of the thickness in the radial direction. The mixed-mode stress intensity factors along the crack front are determined from 3-D conservation integrals, and unlike the case of symmetrical loading, their magnitudes are greater towards the free surface. Near the intersection of the crack front and free surface, the stress field converges to the antisymmetrical corner singularity solution. The asymptotic form of stress near the intersection under general loading conditions is presented, along with the corner stress intensity factors.

1. INTRODUCTION

In a thin plate containing a through-crack, a nearly plane stress condition exists everywhere, except in regions near the crack front, where the state of stress is three-dimensional. In a previous study (Nakamura and Parks, 1988), we considered the near crack front region of a thin plate remotely subjected to Mode I in-plane symmetrical loading conditions. A thin plate is defined as a cracked plate which contains an annular region, outside the near crack front 3-D field, where deformation is essentially characterized by a plane stress K-field solution. Under such conditions, the near crack front field is independent of any *in-plane* dimensions, and the magnitude of loading can be conveniently given by the remote stress intensity factor. The Mode I analysis revealed strong three-dimensionality in the stress field within the radius of about one-half thickness from the tip, and a "2-D–3-D" transitional state persisted up to the radial distance of approximately 1.5 times the thickness of plate. In addition, we have determined that the plane strain $1/\sqrt{r}$ stress field dominates within the radial distance of about 0.5% of the thickness from the tip along the mid-plane of the plate. Furthermore, the corner singularity field was observed near the intersection of crack front and the free surface, and its size was inferred from the behavior of local K.

In the present analysis, the same geometry used in the Mode I analysis (similar to that used by Levy *et al.*, 1971) is adopted to study the 3-D field near a through-crack front in a thin isotropic elastic plate remotely subjected to Mode II in-plane antisymmetrical loading conditions. The thin plate assumptions made in the Mode I analysis are again used for this analysis, so that the near tip region of a plate can be represented by a circular disk which contains a crack front at its center. The model has a sufficiently large radial extent relative to the plate thickness, and its external strip of boundary is subjected to the traction of an assumed surrounding plane stress Mode II K-field. Under these conditions, the "3-D effects" should be confined well within the model, so that the plate thickness is the only characteristic dimension in the region close to the crack front. Although the remote field is plane stress Mode II, the asymptotic stress field along the crack front is expected to be mixed-mode, composed of in-plane Mode II and out-of-plane Mode III, antisymmetrical fields. The out-of-plane deformation occurs due to Poisson expansion/contraction of the plate above/below the crack plane. In order to clarify the mixed-mode K-field very close to the crack front, we introduce two mixity parameters representing the relative strength of each stress intensity factor. The purpose of this study is to assess the size of the 3-D field with respect to the physical scale and to determine characteristic features of the stress field along the crack front under remote in-plane antisymmetrical loading. Furthermore, we investigate the distributions of *local* J and mixed-mode stress intensity factors, K_{II} and K_{III}, and through-thickness for various Poisson's ratios. The values of these fracture-characterizing parameters are obtained from finite element results using appropriate forms of conservation and domain integrals.

Attention is again given to the field near the intersection of the crack front and free surface. We examine the existence and size of a corner singularity field. Here we refer to the works of Bažant and Estenssoro (1979) and Benthem (1980), who studied the asymptotic antisymmetrical singular stress field near the normal intersection/vertex of a crack front and free surface. Our computed results are compared with the solutions given by Benthem (1980), who employed a finite difference scheme to analyze the stress field of a quarter-infinite crack in a half-space. We will also comment on two corner stress intensity factors, symmetrical and antisymmetrical, which represent the amplitudes of singularity fields near the intersection. Finally, general limiting values of a mixity parameter giving the ratio of K_{III} to K_{II} at the corner will be discussed.

2. CRACK TIP FIELD UNDER GENERAL LOADING CONDITIONS

2.1. 3-*D singular stress field*

In an isotropic linear elastic body containing a crack, the stress field very close to the crack front under general (mixed-mode) loading condition is expressed as

$$\sigma_{ij}(r,\theta) = \frac{1}{\sqrt{2\pi r}}\,[K_I f^{I}_{ij}(\theta) + K_{II} f^{II}_{ij}(\theta) + K_{III} f^{III}_{ij}(\theta)], \tag{1}$$

where r and θ are the local polar coordinates in a plane which perpendicularly intersects the crack front at an arbitrary point, and K_I, K_{II} and K_{III} are the local stress intensity factors (at the point) for the opening, sliding and tearing modes, respectively. The functions f^{I}_{ij} and f^{II}_{ij} are the Cartesian components of the *plane strain* asymptotic angular distributions of stress for Modes I and II, respectively, and f^{III}_{ij} are the corresponding components of the asymptotic angular stress distribution for Mode III. It is assumed that the asymptotic stress field (1) exists anywhere along a smooth crack front. An exception may be at a corner point where the crack front meets a free surface (see Section 3.4).

Based on energy release arguments, the relationship between J and the stress intensity factors is

$$J = \frac{(1-\nu^2)}{E}[K_I^2 + K_{II}^2] + \frac{(1+\nu)}{E}K_{III}^2. \tag{2}$$

Here E is Young's modulus and ν is Poisson's ratio.

In a 2-D mixed-mode analysis, Shih (1974) introduced a mixity parameter which is useful in representing the relative strengths of Mode I and Mode II fields. Shih defined a non-dimensional elastic mixity parameter M as

$$M = \frac{2}{\pi}\tan^{-1}\left|\frac{K_I}{K_{II}}\right|. \tag{3}$$

A pure Mode I corresponds to $M = 1$, while a pure Mode II condition is represented by $M = 0$.

The concept of a mixity parameter is extended to the 3-D crack under general loading conditions. Here it is necessary to define two mixity parameters. First we introduce dimensionless parameters $\alpha = \sqrt{1-\nu^2}$ and $\beta = \sqrt{1+\nu}$. Then we imagine a coordinate system made by three orthogonal axes: αK_{I}, αK_{II} and βK_{III}. These axes have the dimension of $[\sigma \cdot l^{1/2}]$ (σ: stress; l: length). Using (2), the length of a vector from the origin to a point in such a coordinate space (spherical radius) equals $\sqrt{EJ}$. Thus, values of stress intensity factors can be conveniently deduced from J and two mixity parameters. The two elastic mixity parameters may be defined from standard spherical angles representing the directions of the vector as

$$M_{\phi} = \frac{2}{\pi}\tan^{-1}\left|\frac{K_{\text{II}}}{K_{\text{I}}}\right|, \quad M_{\theta} = \frac{2}{\pi}\cos^{-1}\left|\frac{\beta K_{\text{III}}}{\sqrt{\alpha^2 K_{\text{I}}^2 + \alpha^2 K_{\text{II}}^2 + \beta^2 K_{\text{III}}^2}}\right|. \tag{4}$$

The first mixity, M_{ϕ}, equals $(1-M)$, where M is Shih's mixity parameter as given in (3). The mixity parameters in (4) represent the relative strengths of the three stress intensity factors. The factor $2/\pi$ is added so that under pure Mode I, II and III conditions, the mixity combinations are $(M_{\phi}, M_{\theta}) = (0, 1)$, $(1, 1)$ and $(*, 0)$, respectively. (Under pure Mode III, M_{ϕ} is undefined.)

2.2. *Three-dimensional J integral and stress intensity factors*

The J integral is a useful parameter in characterizing crack tip fields. In elastic materials, it is equal to the energy release rate and relates to the local stress intensity factors through (2). The local energy release rate J can be expressed in terms of near-tip fields for three-dimensional problems as

$$J^{\text{local}}(s) = \lim_{\Gamma \to 0} \mu_k(s) \int_{\Gamma(s)} \left(W n_k - \sigma_{ij} n_j \frac{\partial u_i}{\partial x_k} \right) \mathrm{d}\Gamma. \tag{5}$$

Here the superscript "local" distinguishes J from a *pointwise* value along a three-dimensional crack front, and s is an arc length measuring the parameter representing the location of the crack tip on the crack front. The strain energy density is W, σ_{ij} and u_i are the Cartesian components of stress and displacement, and n_i are the components of a unit vector normal to Γ and to the crack front tangent vector at s. A path Γ where the integral is evaluated surrounds the crack front at s and lies in the plane perpendicular to crack front, as shown in Fig. 1(a). The Cartesian components $\mu_k(s)$ are those of a unit vector giving the direction which is formed by the intersection of the plane normal to the crack front and the plane tangential to the crack plane at s. The integral (5) defines a local energy release rate along any curvilinear crack front in 3-D space. In general, an equivalent path-independent integral does not exist in 3-D fracture geometries, though the shape of path Γ may be arbitrary as it collapses onto the crack tip.

From a discrete computational point of view, expression (5) is not suitable for evaluating values of $J^{\text{local}}(s)$ since an accurate numerical evaluation of limiting fields along the crack front is difficult. A number of alternate forms for energy release rate that are better suited for numerical calculations have been derived. Here the so-called "domain integral formulation" (Li *et al.*, 1985; Nakamura *et al.*, 1989) is briefly outlined.

First we consider the total energy release by the body due to virtual extension of a small crack front segment between the points $(s-\varepsilon)$ and $(s+\varepsilon)$ as shown in Fig. 1(b). Suppose the amount of crack advance is expressed by $q_l(s)\mu_l(s)$. Then, on integrating (5) over this segment and using the divergence theorem, the total energy release can be expressed as

$$\bar{J}(s) = \int_{s-\varepsilon}^{s+\varepsilon} q_l(s')\mu_l(s') J^{\text{local}}(s')\,\mathrm{d}s' = \int_{V(s)} \left[\sigma_{ij} \frac{\partial u_i}{\partial x_k}\frac{\partial q_k}{\partial x_j} - W\frac{\partial q_k}{\partial x_k} \right] \mathrm{d}V, \tag{6}$$

where $V(s)$ is a volume which encloses the crack front segment [see Fig. 1(c)]. The vector

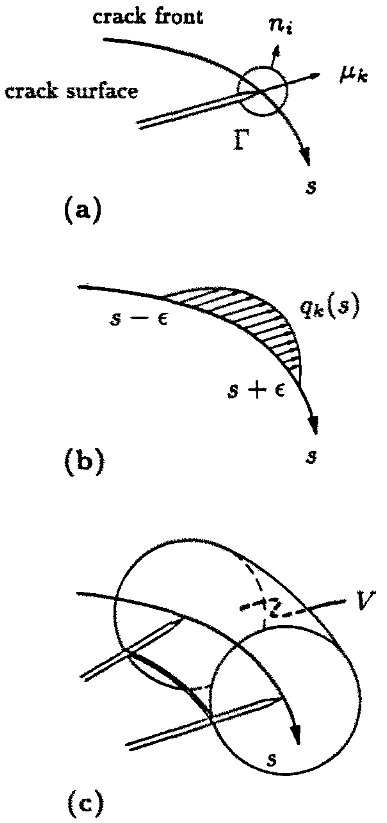

Fig. 1. (a) Crack tip contour Γ on the plane locally perpendicular to the crack front where s is the arc length; (b) virtual crack advance within $s-\varepsilon$ and $s+\varepsilon$ represented by $q_k(s)$; (c) the volume V which encloses the crack front segment.

field q_k is a continuous weighting function of position, and it equals the direction and magnitude of the virtual crack extension for points along the crack front segment [$q_k(s)$ in Fig. 1(b)]. The size of the volume can be arbitrarily chosen, as long as it encompasses the crack front segment and a proper q_k is used. In deriving $\bar{J}$ in (6), the crack faces are assumed to be traction free, and the domain free of body forces, thermal strain, etc.

A simple approximation to J^{local} is obtained by assuming that it is nearly constant within such a crack segment. Then J^{local} can be taken out of the first integral in (6) and solved as

$$J^{\text{local}}(s) = \bar{J}(s) \Big/ \int_{s-\varepsilon}^{s+\varepsilon} q_l(s')\mu_l(s')\,\mathrm{d}s'. \tag{7}$$

A more detailed and consistent procedure for inferring J^{local} from finite element solutions is discussed by Nakamura *et al.* (1989). The computation of the integral over a domain/volume is readily compatible with the finite element formulation, and the domain integral has proven to be a most effective method to compute J in 3-D problems.

In the present analysis, the near-tip field is expected to be composed of both Mode II and Mode III fields. Accurate numerical methods, based on conservation integrals, for extracting the complex stress intensity factor in a mixed-mode 2-D elastic body have been given by Stern *et al.* (1976), Yau *et al.* (1980) and Shih and Asaro (1988). Here we extend these formulations to the general three-dimensional case.

We begin by considering an auxiliary (pseudo) field that is the solution to a crack problem under some arbitrary loads. By superimposing the actual field (the mixed-mode boundary value problem) on the auxiliary field, we can introduce a local interaction energy release rate as

$$I^{\text{local}}(s) = \lim_{\Gamma \to 0} \mu_k(s) \int_{\Gamma(s)} \left[\sigma_{ij}\varepsilon_{ij}^{\text{aux}} n_k - \sigma_{ij} \frac{\partial u_i^{\text{aux}}}{\partial x_k} n_j - \sigma_{ij}^{\text{aux}} \frac{\partial u_i}{\partial x_k} n_j \right] \mathrm{d}\Gamma. \tag{8}$$

Here the variables with the superscript "aux" are the solutions of the auxiliary field. The above integral is a conservation integral as long as the limit ($\Gamma \to 0$) is preserved. Additionally, I^{local} at a point s along the crack front relates to local stress intensity factors of each field by

$$I^{\text{local}}(s) = \frac{(1-\nu^2)}{E}[2K_{\text{I}}K_{\text{I}}^{\text{aux}} + 2K_{\text{II}}K_{\text{II}}^{\text{aux}}] + \frac{(1+\nu)}{E}2K_{\text{III}}K_{\text{III}}^{\text{aux}}, \tag{9}$$

where $K_{\text{I}}^{\text{aux}}$, $K_{\text{II}}^{\text{aux}}$ and $K_{\text{III}}^{\text{aux}}$ are local stress intensity factors for the auxiliary field at a point s. Now suppose we choose the auxiliary field such that the values of its stress intensity factors are $K_{\text{I}}^{\text{aux}} = 1$, $K_{\text{II}}^{\text{aux}} = K_{\text{III}}^{\text{aux}} = 0$ (i.e., a unit plane strain Mode I K-field). Next, we calculate the interaction energy (8) from both the actual and auxiliary field solutions. Then the Mode I component of stress intensity factor, K_{I}, at a point s on the crack front can be deduced from I^{local} through (9) as

$$K_{\text{I}}(s) = \frac{E}{2(1-\nu^2)} I^{\text{local}}(s). \tag{10}$$

This procedure can be repeated for extracting K_{II} and K_{III} by choosing the corresponding auxiliary fields to be the Mode II and III singular field solutions, respectively, and using (9) after each $I^{\text{local}}(s)$ is evaluated through (8).

In order to compute the interaction energy release rate from the finite element results accurately, we follow the domain integral method discussed before. Again we consider the total interaction energy release due to virtual extension of a small crack front segment as shown in Fig. 1(b). With the aids of the weighting function q_k and the divergence theorem, this energy can be expressed in a domain/volume integral form as

$$\begin{aligned} \bar{I}(s) &= \int_{s-\varepsilon}^{s+\varepsilon} q_l(s')\mu_l(s') I^{\text{local}}(s')\,\mathrm{d}s' \\ &= \int_{V(s)} \left[\left(\sigma_{ij} \frac{\partial u_i^{\text{aux}}}{\partial x_k} + \sigma_{ij}^{\text{aux}} \frac{\partial u_i}{\partial x_k} \right) \frac{\partial q_k}{\partial x_j} - \sigma_{ij}\varepsilon_{ij}^{\text{aux}} \frac{\partial q_k}{\partial x_k} \right] \mathrm{d}V. \end{aligned} \tag{11}$$

Here we have used the relation $\sigma_{ij}^{\text{aux}}\varepsilon_{ij} = C_{ijkl}\varepsilon_{kl}^{\text{aux}}\varepsilon_{ij} = \sigma_{kl}\varepsilon_{kl}^{\text{aux}}$, where C_{ijkl} are the Cartesian components of the fourth-order elastic modulus tensor. Again, traction-free crack faces, etc., are assumed. The local interaction energy release rate can be approximated from $\bar{I}$ using a form similar to (7). In this analysis, however, we compute J^{local} and I^{local} using a formulation more consistent with the finite element method (see Nakamura *et al.*, 1989).

3. COMPUTATIONAL ANALYSIS

3.1. *Computational procedure*

The near-tip region of an antisymmetrically loaded thin plate of thickness t [Fig. 2(a)] is modeled by a circular disk (cylinder) shown in Fig. 2(b). The straight crack front is located at the center of the disk along the x_3-axis ($x_1, x_2 = 0$). The maximum radial extent of the disk is five times the thickness ($r_{\max}/t = 5$), which is large enough to contain three-dimensional aspects of the fields within the outer boundary. (This was verified by obtaining plane stress K_{II}-field solutions at $r/t = 5$ using a mesh with a much larger radius.) The external strip of boundary is subjected to the traction of an assumed far-field pure Mode II stress intensity solution.

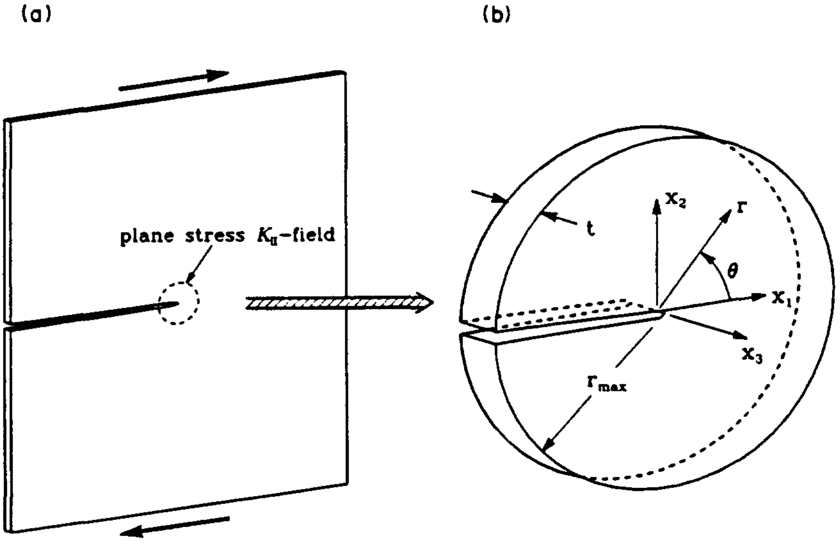

Fig. 2. (a) Schematic of a thin plate subjected to in-plane antisymmetrical loads. A boundary of assumed plane stress K_{II}-field-dominated region is indicated. (b) A cracked circular disk which represents the near crack front region of a thin plate. Cartesian and cylindrical coordinates are indicated.

In constructing the finite element mesh, we have used the elastic linearity and antisymmetrical conditions across the crack and ligament plane ($x_2 = 0$) to model only the upper part of the body. Additionally, the problem possesses reflective symmetry with respect to the mid-plane ($x_3 = 0$), so that only a quarter of the circular disk [region $0 \leqslant \theta \leqslant \pi$, $0 \leqslant x_3/t \leqslant 1/2$, where $\theta = \tan^{-1}(x_2/x_1)$] needs to be modeled. Zero displacement boundary conditions in the x_1 and x_3 directions are prescribed on the ligament portion of the $x_2 = 0$ plane, as well as in the x_3 direction on the $x_3 = 0$ plane. The finite element mesh of this geometry is constructed with 8-node trilinear hexahedron (brick) elements as shown in Fig. 3. In the plane perpendicular to the crack front (x_1–x_2 plane), the element size is gradually increased with radial distance r (where $r = \sqrt{x_1^2+x_2^2}$) from the crack tip, while the angular increment of each element is kept constant, $\Delta\theta = \pi/36$, throughout the mesh. The identical planar mesh is repeated along the x_3-axis from the symmetry plane ($x_3 = 0$) to the free surface ($x_3/t = 1/2$). To accommodate the strong variations of field quantities with respect to the x_3-axis, the thickness of successive element layers is gradually reduced toward the free surface.

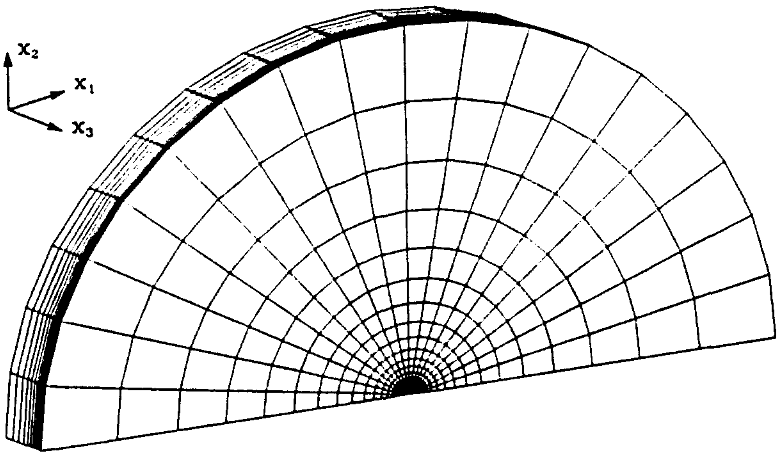

Fig. 3. Finite element mesh of the quarter-model. The front plane corresponds to the free surface.

In carrying out the present analyses, two finite element meshes are employed for each Poisson's ratio considered. The first mesh models the entire radius (up to $r = r_{\max}$), with the plane stress traction boundary condition applied on the outer perimeter (Fig. 3). The second mesh has the same thickness and a similar element arrangement, but the radial extent is a fraction of the first mesh. Within that radius, elements of even smaller radial extent are contained. This finer mesh is used to obtain more accurate solutions near the crack front and near the intersection of the crack front and the free surface. In order to prescribe the boundary condition on the outer perimeter of the finer mesh, the computed displacements from the coarser mesh are interpolated to the boundary nodal points of the finer mesh. The first (coarser) mesh has a total of 5400 elements (18 circumferential × 25 radial in-plane; 12 layers through half-thickness) and 6422 nodes. The second (finer) mesh has 4860 elements (18 × 18 in-plane; 15 layers through half-thickness) and 5776 nodes. The radial extent of the outermost nodes of the second mesh is $0.181t$, its crack tip elements have a radial extent of $0.001t$, and the thickness of the element layer adjoining its free surface is $0.002t$. The crack front is surrounded by wedge-shaped elements whose inner nodes are collapsed to share the same coordinate but have independent degrees of freedom. At each crack front location, the zero boundary conditions in the x_1 and x_3 directions are imposed only on the crack front node which is part of the ligament plane.

The traction boundary condition was applied to the first mesh by computing consistent nodal forces. The plane stress $K_{\rm II}$-field traction, weighted by nodal shape functions, was integrated over each element's surface. The stress distribution on the outer boundary is given by

$$\sigma_{ij} = \frac{K_{\rm II}^{\rm far}}{\sqrt{2\pi r_{\max}}} f_{ij}^{\rm II}(\theta). \tag{12}$$

Here $K_{\rm II}^{\rm far}$ is the assumed far-field (remote) Mode II stress intensity factor and $f_{ij}^{\rm II}$ are the *plane stress* components of angular distribution of stress.

The material behavior of the plate is taken to be isotropic linear elastic. In our computation, Poisson's ratios of $\nu = 0$, 0.15, 0.30, 0.40 and 0.499 were chosen.

All the finte element results were obtained using the finite element code ABAQUS (1987); the calculations were carried out on an Alliant FX-8 computer. To alleviate the potential numerical difficulties associated with the nearly incompressible solid ($\nu = 0.499$), the B-bar method (Nagtegaal *et al.*, 1974; Hughes, 1980) was implemented in the program for the formulation of the element stiffness matrices. In the case of the 8-node brick element, the volumetric components of the strain/displacement **B** matrix were obtained by 1-point quadrature, while the deviatoric components were obtained by 2 × 2 × 2 Gaussian quadrature. The former integration results in a uniform hydrostatic pressure throughout the element. As a safeguard against spurious pressure modes, we employed the modified **B**-bar method discussed in Nakamura *et al.* (1989). A small weighting factor of 0.0001 was chosen for our analyses. This method was employed for all the Poisson's ratios in order to obtain consistency in the computations.

3.2. *Three-dimensional field of thin plate*

The deformation field in a thin plate was nearly uniform through-thickness, except in the region near the crack front. The transition to the three-dimensional state occurs within a radial distance from the crack front of the order of the plate thickness. In order to show the general features of the 3-D antisymmetrical field, the in-plane shearing stress ahead of crack front ($\theta = 5^\circ$) for each Poisson's ratio is plotted as a function of radial distance in Fig. 4(a). The stress is normalized by the corresponding component of the far-field plane stress solution, eqn (12). In this figure, *mid-plane* and *edge-plane* denote the element layer closest to the mid-plane or symmetry-plane and the element layer adjoining the free surface, respectively. The stress output is given at the centroid of each element, along $x_3/t = 0.05$ for the mid-plane and $x_3/t = 0.495$ for the edge-plane. The curves in Fig. 4(a) show the computed stress to be nearly identical with the plane stress value for all Poisson's ratios at

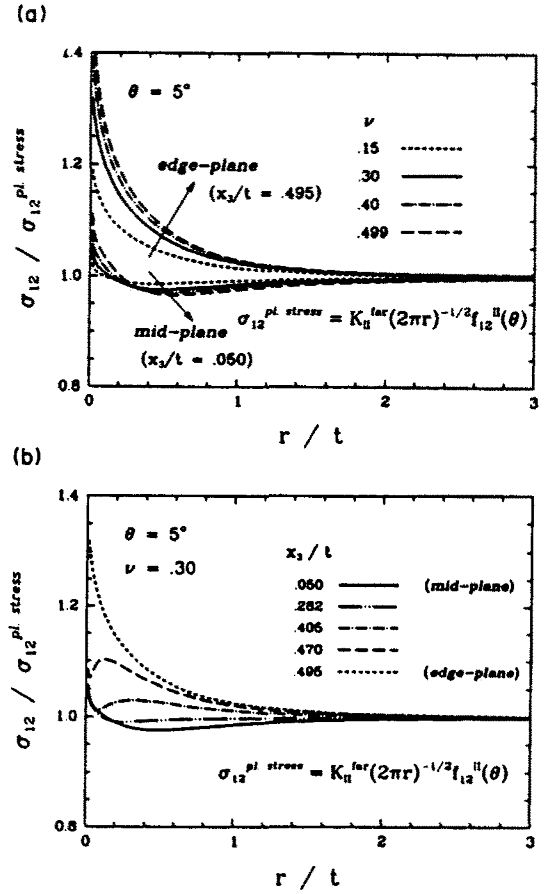

Fig. 4. Shear stress ahead of crack front normalized by corresponding component of 2-D plane stress K_{II}-field solution; (a) for various Poisson's ratios at mid-plane and edge-plane; (b) for $\nu = 0.30$ at different depths. (Note zero suppression of ordinate axis.)

large r/t. At smaller r/t, the difference between the mid-plane and the edge-plane values increases. Also, the differences between complete and two-dimensional solutions are greater at the edge-plane than at the mid-plane, and the results of higher Poisson's ratios have larger amplitude of variation through-thickness. In any case, unlike the behavior of opening stress observed in the Mode I analysis, the shearing stress near the crack front is higher at the edge-plane than at the mid-plane. The stress at different depths in the plate for $\nu = 0.30$ is plotted in Fig. 4(b). Again, it generally appears that the stress increases towards the edge-plane near the crack front. This feature is more clearly illustrated by the variation of K_{II} through-thickness shown below. These figures show that the small deviation from two-dimensionality (uniform through-thickness) starts near $r/t = 1.5$, and that within $r/t < 0.5$, the three-dimensionality of the stress field is significant.

In our previous analysis of symmetrical loading of a thin cracked plate, we noted that certain features of the 2-D plane stress → 3-D transitional field could be captured by an approximate 3-D stress function based on the underlying plane stress solution (Nakamura and Parks, 1988). The application of that procedure to the present case gives

$$\frac{\sigma_{12}^{\text{approx}}}{\sigma_{12}^{\text{pl. stress}}} = 1+\frac{3}{4}\,\frac{\nu}{1+\nu}\left(\frac{x_3}{r}\right)^2 \cos\frac{5\theta}{2}\Big/\cos\frac{\theta}{2}\left(1-\sin\frac{\theta}{2}\sin\frac{3\theta}{2}\right). \tag{13}$$

The results shown in Fig. 4 are in good qualitative agreement with (13) in the region $r/t \gtrsim 1$; e.g. small stress variation at mid-plane, increasing stress with increasing distance from mid-plane, with larger stress variation at higher Poisson ratio.

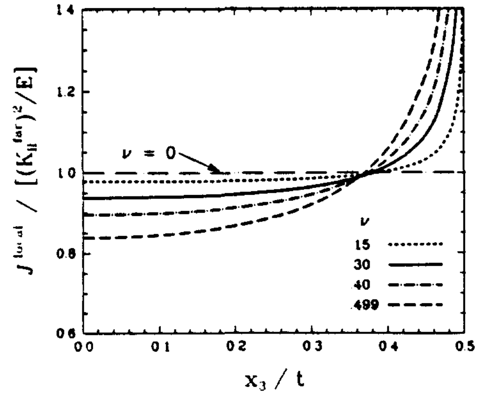

Fig. 5. Normalized local J along the half-crack front for various Poisson's ratios. (Note zero suppression of ordinate axis.)

The size of the three-dimensional field was also investigated from other components of stress and displacement at various locations, including the out-of-plane displacement, u_3, and the degree of plane strain, $\sigma_{33}/\nu(\sigma_{11}+\sigma_{22})$. Qualitatively, the results of these variables are nearly identical to the ones shown in the symmetrical field analysis (Nakamura and Parks, 1988). They confirm similar characteristics of the near crack front 3-D field—a gradual change from the far-field plane stress condition occurs near the radial distance of $1.5t$ from the crack tip, and a significant increase in through-thickness variation of field quantities is observed within $r/t < 0.5$. The size of the 3-D field appears to be independent of Poisson's ratio (except $\nu = 0$).

The J integral along the crack front is obtained using the domain integral method described in Section 2.2. The values of local J inferred from different domains are generally within 0.5% of the mean value at each nodal location along the crack front, except for the free surface position, where the domain dependence is somewhat larger. At each location, the mean J value over the domains is denoted as J^{local}. Identical distributions of J are obtained from the initial mesh and the second (finer) mesh, except that more detailed results near the free surface are observed from the finer mesh. This justifies the method used to obtain accurate solutions near the crack front and free surface. The variation of J^{local} along the crack front is shown in Fig. 5 for different Poisson's ratios. The local J is normalized by $(K_{II}^{\text{far}})^2/E$, which is also the value of the average J for the entire crack front. The figure shows an exactly opposite trend from the familiar Mode I results. The computed J^{local} in the antisymmetrical field shows the minimum values at the symmetry-plane ($x_3/t = 0$) and the maximum values on the free surface ($x_3/t = 0.5$) for all the non-zero Poisson's ratios. In fact, J^{local} increases very rapidly toward the free surface. This behavior is consistent with the corner singularity solution which is discussed in Section 3.4. The result for $\nu = 0$ is identical to the 2-D solution with the same Poisson's ratio. Interestingly, all the curves pass through (near) a point located at $x_3/t = 0.36$ and $J^{\text{local}}/[(K_{II}^{\text{far}})^2/E] = 1$.

Figure 6 shows the variation through-thickness of local stress intensity factors. Each factor is denoted with superscript "local" to distinguish from the far-field/remote stress intensity factor. These values are obtained from $\bar{I}$ in (11), where the auxiliary field is set to the $1/\sqrt{r}$ plane strain Mode II solution for extracting K_{II}^{local}, and to the $1/\sqrt{r}$ Mode III solution for extracting K_{III}^{local}. Since our mesh models only the upper half of the plate, antisymmetrical terms in (11) are properly accommodated in computing $\bar{I}$ over the entire domain V. The Mode II stress intensity factor K_{II}^{local}, as shown in Fig. 6(a), remains constant over nearly the entire crack front and increases rapidly near the free surface (except that for $\nu = 0$). In Fig. 6(b), the Mode III stress intensity factor K_{III}^{local} is shown. Since the out-of-plane displacement is antisymmetrical across the plane $x_3/t = 0$, K_{III}^{local} is an odd function of x_3 and vanishes at $x_3/t = 0$. Again, unlike the K_{I}^{local} seen in the Mode I analysis, the (absolute) value of K_{III}^{local} increases monotonically for larger x_3/t and appears to approach infinity at the free surface. The local J at nodal points along the crack front are computed from K_{II}^{local} and K_{III}^{local} using relation (2). The values are within 1% of J^{local} shown in Fig. 5

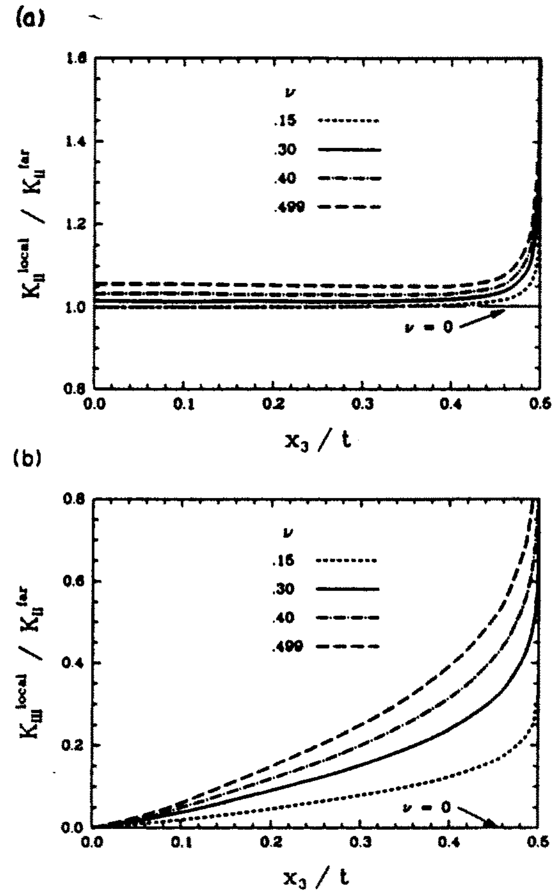

Fig. 6. Normalized local stress intensity factor components along the half-crack front for various Poisson's ratios; (a) for Mode II component (note zero suppression of ordinate axis); (b) for Mode III component.

(except at the free surface node), further substantiating the accuracy of these parameters obtained through the domain integrals.

In Fig. 7 we have plotted the local mixity factor M_θ of (4). Since the field is antisymmetrical and $K_I^{\text{local}} = 0$ (K_{II}^{local} is never zero in the present case), the other mixity parameter is unity ($M_\phi = 1$) through-thickness. With this condition, M_θ depends only on K_{II}^{local} and K_{III}^{local}; $M_\theta = 1$ corresponds to pure Mode II while $M_\theta = 0$ corresponds to pure Mode III. The curves in Fig. 7 show pure Mode II at the symmetry-plane ($x_3/t = 0$) and decreasing values of M_θ towards the free surface for all values of ν. Since the Mode III

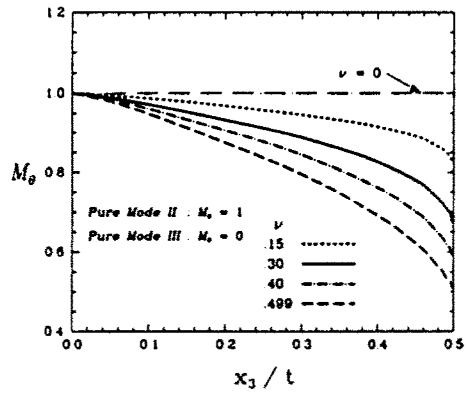

Fig. 7. Mixity parameter M_θ along crack front. In antisymmetrical fields, the other mixity parameter M_ϕ is unity. (Note zero suppression of ordinate axis.)

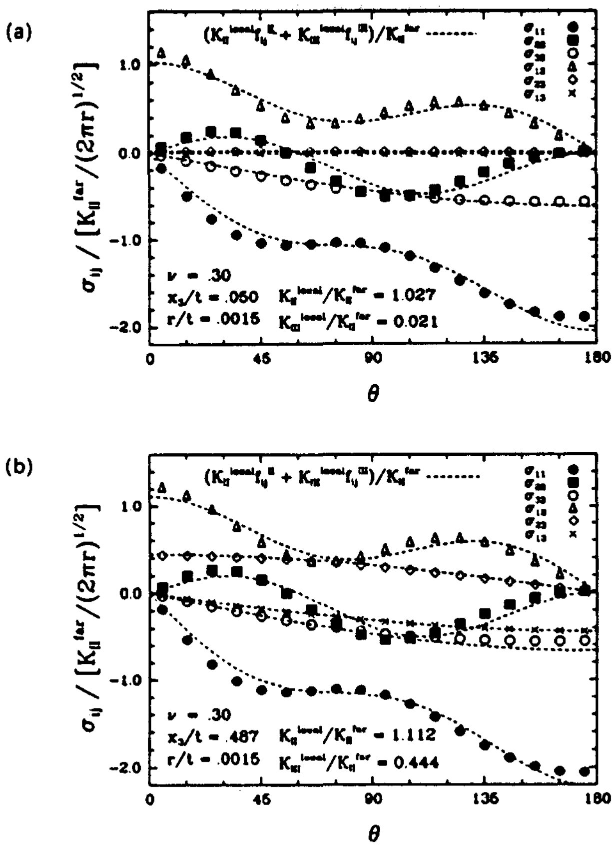

Fig. 8. Angular distributions of stress components very near crack front normalized by K_{II}^{far}; (a) at $x_3/t = 0.050$, where $K_{II}^{local}/K_{II}^{far} = 1.027$ and $K_{III}^{local}/K_{II}^{far} = 0.021$; (b) at $x_3/t = 0.487$, where $K_{II}^{local}/K_{II}^{far} = 1.112$ and $K_{III}^{local}/K_{II}^{far} = 0.444$. In both figures, appropriately weighted corresponding 2-D angular stress distributions are shown with dashed lines for comparison.

contribution is due to the Poisson's effect of the material, the relative strength of K_{III}^{local} is greater for larger values of ν.

3.3. *Near-tip asymptotic condition*

If the normal out-of-plane strain component, ε_{33}, is bounded or less singular than $1/\sqrt{r}$ along the crack front, then a *pointwise* two-dimensional condition should emerge as the crack front is approached. Thus, asymptotically, a $1/\sqrt{r}$ singular stress solution (1) will prevail near the crack front. The behavior of this strain component is very similar to that obtained in the previous Mode I analysis. For very small r/t the relative value of ε_{33} (as compared to a norm of in-plane strain components) approaches zero in almost identical manner for all the non-zero Poisson's ratios.

The complete stress field very near the crack tip ($r/t = 0.0015$) is shown in Fig. 8. The components of computed stress are normalized by K_{II}^{far} and are plotted over the angular range $0 < \theta < \pi$ for $\nu = 0.30$. The angular distributions f_{ij}^{II} and f_{ij}^{III} of (1) are shown with dashed lines. Since the field is a mixture of Modes II and III, these functions are weighted by respective local stress intensity factors obtained earlier from the domain integrals. For each stress component, Fig. 8(a) shows good agreement between the computed stress and the 2-D solution at the mid-plane, $x_3/t = 0.050$. The values of K_{II}^{local} and K_{III}^{local} at this crack front location are indicated in the figure. In Fig. 8(b), the same variables are similarly plotted near the free surface, $x_3/t = 0.487$, where there is a much greater Mode III influence. These results confirm the assertion that the asymptotic stress field along a crack front is indeed characterized by singular K-field solutions as in (1).

The agreement with the local K-field solution deteriorates as the radial distance from the crack front increases. The deterioration is most evident in the decay of σ_{33} from the plane strain constraint. Based on comparisons of the complete and asymptotic solutions, we conclude that K-fields (mixed-mode) exist along the 3-D crack front within the radius of approximately $0.005t$ for a thin plate under general loading conditions, similar to that found in the Mode I analysis.

3.4. *Corner singularity field*

At a point sufficiently close to the normal intersection of crack front and free surface, the asymptotic deformation field should be characterized by the corner singularity field of a quarter-infinite crack plane in a half-space. According to Benthem (1977), the stress in the corner singularity field may be expressed in a separable form as

$$\sigma_{ij} \propto \rho^{\lambda} g_{ij}(\theta, \phi), \tag{14}$$

where λ is the coefficient of stress singularity, g_{ij} is a dimensionless angular function depending on the Poisson's ratio, and spherical coordinates centered at the vertex are

$$\rho = \sqrt{r^2 + z^2}, \quad \phi = \tan^{-1}\left(\frac{r}{z}\right), \quad z = \frac{t}{2} - x_3. \tag{15}$$

This asymptotic form was also shown by Bažant and Estenssoro (1979). In a previous analysis of the symmetrical corner field, Nakamura and Parks (1988) introduced the corner stress intensity factor, $\mathscr{B}$, as a scaling constant in eqn (14). Furthermore, its relationship with the local stress intensity factor near the intersection was shown to be

$$K^{\text{local}}(z) = \mathscr{B} z^{\lambda + 1/2} \quad \text{for} \quad z \to 0. \tag{16}$$

Here $\mathscr{B}$ has the dimension $[\sigma \cdot l^{-\lambda}]$ (σ: stress; l: length dimensions). Using a similar idea, the stress field under more general loading conditions can be given in terms of a complex corner stress intensity factor. For mixed-mode fields, the stress near the intersection may be expressed in terms of dominant symmetrical and antisymmetrical corner singularities as

$$\sigma_{ij}(\rho, \theta, \phi) = \frac{1}{\sqrt{2\pi}} [\mathscr{B}_S \rho^{\lambda_S} g_{ij}^S(\theta, \phi) + \mathscr{B}_A \rho^{\lambda_A} g_{ij}^A(\theta, \phi)]. \tag{17}$$

Here $\mathscr{B}_S$ [same as $\mathscr{B}$ in (16)] and $\mathscr{B}_A$ are the corner stress intensity factors corresponding to the symmetrical and antisymmetrical fields, respectively. Also, λ_S is the eigenvalue for symmetrical fields, and λ_A is the eigenvalue for antisymmetrical fields. The leading roots range over $-0.5 \leqslant \lambda_S \leqslant -0.332$ and $-0.5 \geqslant \lambda_A \geqslant -0.646$ for $0 \leqslant \nu \leqslant 0.5$, respectively (Benthem, 1977, 1980; Bažant and Estenssoro, 1979). The dimensionless angular functions g_{ij}^S and g_{ij}^A also depend on ν. For $\nu \neq 0$, these values of λ suggest that the second term in (17) dominates as $\rho \to 0$ under *any* mixed-mode conditions, and in general, the asymptotic field is pure antisymmetrical at the intersection. On the free surface ($\phi = 90°$), $\rho = r$, and the stress singularity (in r) is more severe than the $1/\sqrt{r}$ singularity observed within the interior of plate, except when the local stress field is exactly symmetrical.

A complete relationship between the stress intensity factors and the corner stress intensity factors can be expressed in a fashion similar to (16) as

$$\begin{aligned} K_{\text{I}}^{\text{local}}(z) &= \mathscr{B}_S z^{\lambda_S + 1/2} \\ K_{\text{II}}^{\text{local}}(z) &= \mathscr{B}_A z^{\lambda_A + 1/2} \qquad \text{for} \quad z \to 0. \\ K_{\text{III}}^{\text{local}}(z) &= R(\nu)\mathscr{B}_A z^{\lambda_A + 1/2}. \end{aligned} \tag{18}$$

Here $R(\nu)$ is a dimensionless factor equivalent to the ratio of $K_{\text{III}}^{\text{local}}$ to $K_{\text{II}}^{\text{local}}$, and it is a function of *only* Poisson's ratio. Equations (18) suggest that the local stress intensity factor tends to zero in a symmetrical field and tends to infinity in an antisymmetrical field for

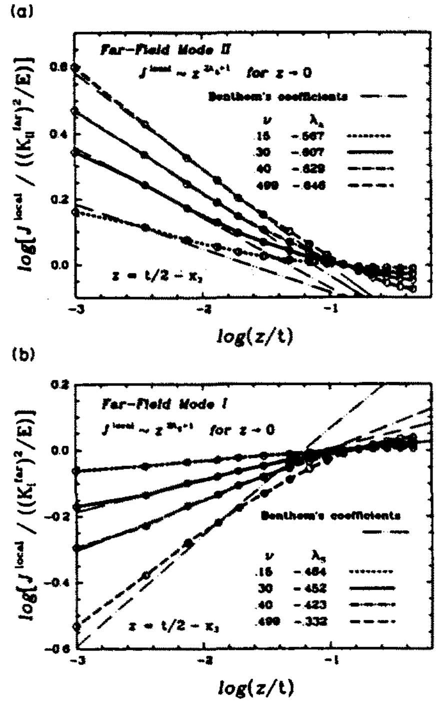

Fig. 9. Normalized J^{local} for various Poisson's ratios plotted against normalized distance from the intersection on a log–log scale. Small circles represent the mid-location of element layers along the crack front. Benthem's singularity exponents are shown in the inset. Also, slopes of straight lines correspond to the corner singularity field solutions. (a) For antisymmetrical fields under far-field Mode II. (b) For symmetrical fields under far-field Mode I.

small z and $\nu \neq 0$ (see Fig. 6). From (1), (17) and (18), we can also determine the relationships between angular functions f_{ij} and g_{ij} to be

$$f^{\rm I}_{ij}(\theta) = \lim_{\phi \to 0} \sqrt{\phi}\, g^{\rm S}_{ij}(\theta, \phi) \qquad f^{\rm II}_{ij}(\theta) + R(\nu) f^{\rm III}_{ij}(\theta) = \lim_{\phi \to 0} \sqrt{\phi}\, g^{\rm A}_{ij}(\theta, \phi). \tag{19}$$

Here $f^{\rm I}_{ij}(\theta)$, $f^{\rm II}_{ij}(\theta)$ and $f^{\rm III}_{ij}(\theta)$ are the plane strain Mode I and II and anti-plane Mode III angular distribution of stress given in (1), and, unlike the functions g_{ij}, they are independent of ν.

In order to determine the dominance of such corner singularity field in a finite thickness plate, J^{local} was plotted on a log–log scale in Fig. 9(a). The computed value of J^{local} was employed since it is expected to be more accurate than K^{local}_{II} or K^{local}_{III} near the free surface. If (18) holds true near the free surface of the thin plate, J^{local} should be proportional to $z^{2\lambda_A+1}$ for small z [from (2)]. The small circles in the figure indicate J^{local} at the mid-locations of element layers along the crack front, and the tangent of each curve corresponds to the exponent of z. Also plotted in the figure are the straight lines whose slopes are $2(\lambda_A + 1/2)$ for the respective Poisson's ratios. The values of λ_A given by Benthem are depicted in the inset. The curves are nearly straight for $z/t < 0.03$, and the agreement with Benthem's solutions is very good for all the Poisson's ratios. A similar figure is shown in Fig. 9(b) from results of the Mode I analysis (Nakamura and Parks, 1988) for reference. Based on the behaviors of J near a corner as shown in Fig. 9, we tentatively conclude that the corner singularity field in a thin plate dominates within the spherical radius of $\rho/t \simeq 0.03$ from the intersection for all the (non-zero) Poisson's ratios and both symmetrical and antisymmetrical fields.

From the computed values of local stress intensity factor very near the intersection ($z/t < 0.03$), we can determine the amplitude of corner stress intensity factor for a thin plate using (18). The factor $\mathscr{B}_A$, normalized with K^{far}_{II} and $t^{\lambda_A+1/2}$, is plotted as a function of ν in

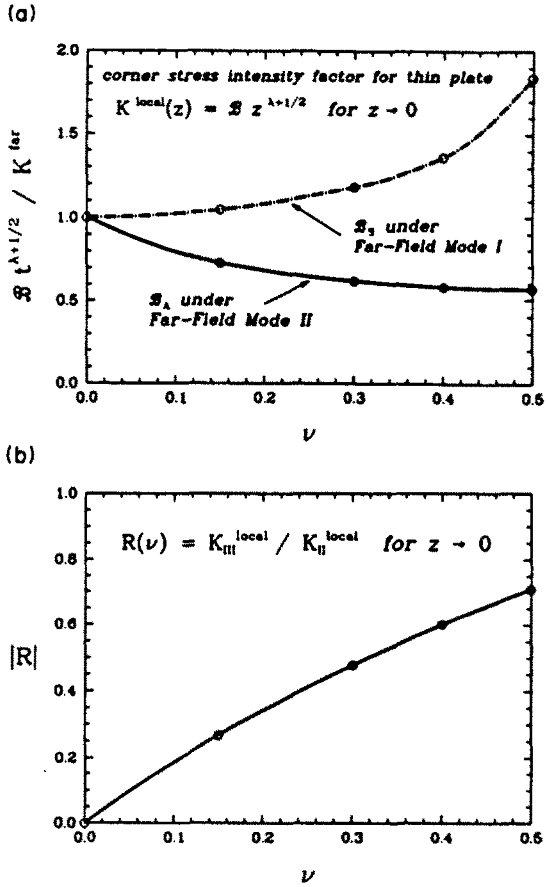

Fig. 10. (a) Components of corner stress intensity factor, $\mathscr{B}_A$, for a thin plane under far-field in-plane antisymmetrical load, normalized with K_{II}^{far} and shown as a function of Poisson's ratio, ν. Also $\mathscr{B}_S$ from Nakamura and Parks (1988) is shown for reference. (b) The ratio of K_{III}^{local} to K_{II}^{local}, $R(\nu)$, determined from M_θ in Fig. 7 for $x_3/t \to 1/2$.

Fig. 10(a). These solutions are *universal* in the sense that if a plate satisfies the *thin plate* requirements, they are independent of any in-plane dimensions of the plate. For reference, we have included $\mathscr{B}_S$, normalized with K_I^{far} and $t^{\lambda_S+1/2}$, from the previous analysis, the thin plate under in-plane symmetrical load (far-field Mode I), in the same figure.

As stated by Benthem (1980), Modes II and III cannot occur independently at the intersection, and the ratio of K_{III}^{local} to K_{II}^{local} is fixed for a given Poisson's ratio. [Bažant and Estenssoro (1979) cite a private communication from L. M. Keer as also reaching this conclusion.] For the case of non-normal intersection, the limiting ratio also depends on the crack edge angle and crack plane angle, as indicated in Bažant and Estenssoro (1979). The function $R(\nu)$ may be obtained from the computed local stress intensity factors near the free surface. In terms of the mixity parameter given in (4), it is

$$R(\nu) \to \sqrt{1-\nu} \Big/ \tan\left[\frac{\pi}{2} M_\theta(z;\nu)\right] \quad \text{as} \quad z \to 0. \tag{20}$$

Based on the limiting values of M_θ at $x_3/t = 0.5$ shown in Fig. 7, $R(\nu)$ are determined and plotted in Fig. 10(b). (The sign of R is arbitrary as it depends on the choice of coordinate's direction.) The value given by Benthem (1980), from his stress intensity factors, is $R(\nu) = 0.50$ for $\nu = 0.30$, which is in good agreement with that found here. We emphasize that the relative strength of the Mode II and III stress intensity factors near the corner, while depending on ν, is *independent* of loading conditions. We have also applied other antisymmetrical loading boundary conditions to crack meshes of this sort. While the resulting local fields were quite different in nature, the ratio R or the local mixity parameter M_θ near the corner was always in good agreement with the result shown in Fig. 10(b), further substantiating the generality of the result.

4. DISCUSSION

The results of a thin plate under remote Mode II loading show strong 3-D effects up to a radial distance of approximately half the plate thickness from the crack front and weaker through-thickness variations of stress field within $0.5 < r/t < 1.5$. These values are consistent with the results found in the analysis of a thin plate under Mode I loading.

We have also shown that the asymptotic stress field along the crack front is indeed characterized by the K-field (mixed-mode) solutions, and the corresponding stress intensity factors can be successfully computed from finite element results using the conservation and domain integrals. The domain of such near crack front K-field extends approximately 0.5% of the thickness in the radial direction at the mid-plane. The extracted values of stress intensity factor indicate the magnitude of the $1/\sqrt{r}$ singular field to be greater towards the free surface, a trend completely opposite to the Mode I results. This result may imply that, under antisymmetrical or *any* mixed-mode loading conditions, first fracture initiation occurs at the edge of the crack front (corner point) instead of at a interior location of the plate.

Near the intersection of the crack front and free surface, the computed field approaches the asymptotic antisymmetrical solutions given by Benthem (1980) and Bažant and Estenssoro (1979). The corner stress field under general loading conditions is expressed in terms of symmetrical and antisymmetrical corner stress intensity factors. It appears that the corner singularity field dominates up to the radial distance of 3% of the thickness of a thin plate under any type of loading condition.

At the exact corner point, the standard intensity factors of fracture mechanics lose their meaning, since a $1/\sqrt{r}$ singular field generally does not exist. However, the limiting value of the ratio of K_{III}^{local} to K_{II}^{local} does exist, and it varies depending on ν and on the angles of crack edge and crack plane, as discussed in Bažant and Estenssoro (1979). It is possible to find a crack intersection (edge) angle for a given crack plane angle and Poisson's ratio to have a finite energy release rate and invariant stress intensity factor for small z (Bažant and Estenssoro, 1979). For the present geometry of perpendicular intersecting angle and zero inclined crack plane angle, such a condition occurs when Poisson's ratio is zero.

As long as the antisymmetrical corner stress intensity factor is not zero ($\mathscr{K}_A \neq 0$), the second term dominates in (17), and higher limiting stresses prevail at the corner. This suggests that, if an existing crack front is nearly straight, crack initiation under mixed-mode loading would tend to begin near the intersection of crack front and free surface. Such phenomena were indeed observed in a recent experimental study by Aoki *et al.* (1989), who noted shear crack emanations from the edges under various far-field mixed-mode (I and II) conditions.

In homogeneous plates subject to mode II loading, extended cracking in the initial plane is not expected, as generally the crack will kink out of its prior plane. One case where in-plane "cracking" does occur is the propagation of the slipping/locked boundary along strike-slip faults. Our analysis of a through-crack making an orthogonal intersection with the free surface resulted in extremely large stress intensities near the surface. It is thus natural to assume that, at the surface, an actual slipping boundary would extend further into the locked portion than it would at mid-plate depth, resulting in an unfamiliar (as compared to advancing mode I crack fronts) convex shape. Indeed, Rice (1988) has noted that this interpretation of our results is consistent with seismic and geodetic data at the boundaries (near Parkfield and San Juan Batista, California) of a slipping portion of the San Andreas.

Acknowledgements—The authors gratefully acknowledge the support of D.O.E., through the joint project between M.I.T. and the Idaho National Engineering Laboratories under Grant No. DE-FG02-85ER13331, and of the Department of Mechanical Engineering, S.U.N.Y. at Stony Brook. Computations were performed on an Alliant FX-8 at M.I.T., obtained under DARPA Grant No. N00014-86-K-0768, and on a VAX 8600 at Stony Brook.

The ABAQUS finite element code was made available under academic license from Hibbitt, Karlsson and Sorensen, Inc., Providence, RI.

REFERENCES

ABAQUS (1987). Version 4.6, Hibbitt, Karlsson and Sorensen, Inc., Providence, RI.

Aoki, S., Kishimoto, K., Yoshida, T., Sakata, M. and Richard, H. A. (1989). Elastic-plastic fracture behavior of an aluminum alloy under mixed mode loading. *J. Mech. Phys. Solids*, to appear.

Bažant, Z. P. and Estenssoro, L. F. (1979). Surface singularity and crack propagation. *Int. J. Solids Struct.* **15**, 405–426.

Benthem, J. P. (1977). State of stress at the vertex of a quarter-infinite crack in a half-space. *Int. J. Solids Struct.* **13**, 479–492.

Benthem, J. P. (1980). The quarter-infinite crack in a half-space; alternative and additional solutions. *Int. J. Solids Struct.* **16**, 119–130.

Hughes, T. J. R. (1980). Generalization of selective integration procedures to anisotropic and nonlinear media. *Int. J. Numer. Meth. Engng* **16**, 1413–1418.

Levy, N., Marcal, P. V. and Rice, J. R. (1971). Progress in three-dimensional elastic–plastic stress analysis for fracture mechanics. *Nucl. Engng Des.* **17**, 64–75.

Li, F. Z., Shih, C. F. and Needleman, A. (1985). A comparison of methods for calculating energy release rate. *Eng. Fract. Mech.* **21**, 405–421.

Nagtegaal, J. C., Parks, D. M. and Rice, J. R. (1974). On numerically accurate finite element solutions in the fully plastic range. *Comput. Meth. Appl. Mech. Engng* **4**, 153–178.

Nakamura, T. and Parks, D. M. (1988). Three-dimensional stress field near the crack front of a thin elastic plate. *J. Appl. Mech.* **55**, 805–813.

Nakamura, T., Shih, C. F. and Freund, L. B. (1989). Three-dimensional transient analysis of a dynamically loaded three-point-bend ductile fracture specimen. *ASTM STP* **995**, 217–241.

Rice, J. R. (1988). Private communication to D. M. Parks.

Shih, C. F. (1974). Small-scale yielding analysis of mixed mode plane-strain crack problems. *ASTM STP* **560**, 187–210.

Shih, C. F. and Asaro, R. J. (1988). Elastic–plastic analysis of cracks on bimaterial interfaces; part I: small scale yielding. *J. Appl. Mech.* **55**, 299–316.

Stern, M., Becker, E. B. and Dunham R. S. (1976). A contour integral computation of mixed mode stress intensity factors. *Int. J. Fract.* **12**, 359–368.

Yau, J. F., Wang, S. S. and Corten, H. T. (1980). A mixed mode crack analysis of isotropic solids using conservation laws of elasticity. *J. Appl. Mech.* **47**, 335–341.